applied sciences

MDPI

Article

Research on Lateral Deformation Control Criteria of Metro Shield Tunnels with Excessive Ellipticity

Shaode Kan [1], Junsheng Chen [2,3,*], Yuehua Liang [1], Yizhao Wang [1] and Huanyang Zhou [2]

[1] Guangzhou Metro Design & Research Institute Co., Ltd., Guangzhou 510010, China; kanshaode@gmdi.cn (S.K.); liangyuehua@dtsjy.com (Y.L.); wangyizhao@dtsjy.com (Y.W.)
[2] State Key Laboratory of Subtropical Building Science, School of Civil Engineering and Transportation, South China University of Technology, Guangzhou 510640, China; zhouhy_scut@163.com
[3] South China Institute of Geotechnical Engineering, South China University of Technology, Guangzhou 510640, China
* Correspondence: jschen@scut.edu.cn

Abstract: In recent years, excessive lateral deformation of subway shield tunnels has been observed due to adjacent engineering activities. This study examines the monitoring of excessive lateral deformation of the shield tunnel and the special steel plate reinforcement process to enhance the safety and stability of the operating subway tunnel structure. It uses a three-dimensional refined finite-element model of the shield tunnel for parametric structural loading simulation analysis to propose a structural deformation limit value suitable for the subway shield tunnel. This study's findings indicated the following: (1) as observed from the engineering examples, a tunnel with significant elliptical deformation increases the likelihood of cracking and other structural issues in the adjacent subway shield tunnel segment; (2) as observed from the post-reinforcement monitoring data, the steel plate reinforcement method effectively enhances the load-bearing stability of the damaged tunnel structure; (3) based on the finite-element simulation results and the comprehensive review of practical conditions, the standard warning value for lateral deformation, using ellipticity evaluation of the subway shield tunnel, is established at 20‰, with a control value of 25‰. The outcomes of this research offer valuable insights into the operation, maintenance, and health monitoring of subway shield tunnels.

Keywords: shield tunnel; ellipticity; numerical simulation; deformation control criteria

Citation: Kan, S.; Chen, J.; Liang, Y.; Wang, Y.; Zhou, H. Research on Lateral Deformation Control Criteria of Metro Shield Tunnels with Excessive Ellipticity. *Appl. Sci.* **2023**, *13*, 12721. https://doi.org/10.3390/app132312721

Academic Editor: Tiago Miranda

Received: 18 October 2023
Revised: 10 November 2023
Accepted: 21 November 2023
Published: 27 November 2023

1. Introduction

Over the years, the operational mileage of shield subway tunnels in major cities in China has expanded due to the growth of urban construction. This growth has been accompanied by frequent structural safety challenges attributed to tunnel deformation [1,2]. The earth mounding and pit excavation of adjacent subways can result in significant structural deformation of the tunnel, particularly the prefabricated and assembled shield tunnel segments. Such deformations can lead to structural issues such as water leakage, segment cracking, and roadbed separation [3–6]. The intricacies of engineering geology further add complexities to the daily operation and maintenance of rail transit [7–9].

The prefabricated and assembled nature of subway shield tunnels allows for deformation tolerance. However, excessive lateral deformation can severely disrupt the tunnel's structure and the subway's regular operations. Consequently, the lateral deformation of shield tunnels remains a focal research area in domestic and international shield tunneling sectors. Yamamoto et al. [10,11] used the finite-element method for planar strain analysis to investigate the stability of single-circle and double-circle tunnels in cohesive soils subjected to ground stacking loads. Similarly, Shi et al. [12] developed a hybrid model for shield tunnels based on three-dimensional nonlinear contact theory, outlining deformation control criteria for existing tunnels under lateral unloading. Tian et al. [13] highlighted that the

damage mode of a shield tunnel's segment is influenced by its initial defects. Su et al. [14] utilized finite-element software to create a comprehensive numerical model of the shield tunnel lining, exploring the impact of varying soil loosening degrees and locations on the tunnel's mechanical response. Collectively, these studies emphasized the structural attributes of shield tunnels and the effects of neighboring engineering activities, primarily through the finite-element method. As the primary load-bearing component of the shield tunnel, the reinforced concrete precast segment undergoes various influences during the metro tunnel's operational phase. Although the theoretical method to determine its response involves several simplifications, numerous studies indicate that numerical simulation using the finite-element method is an efficient approach, especially when discussing complex loading scenarios [15–17].

Ellipticity offers a straightforward and readily available monitoring metric for tunnels, providing a clear assessment of the tunnel structure's operational safety and the degree of external influence. However, research on the lateral deformation limits of tunnels based on ellipticity remains limited. This study explores the causes of substantial lateral deformation in shield tunnels and associated structural challenges, using a case of significant lateral deformation in an active underground rail transit as the primary context.

2. Excessive Transverse Deformation Cases in Ghuangzhou Metro

2.1. Introduction to Tunnel Defect Cases

The subway tunnel in Guangzhou is located in a typical upper soft and lower hard stratum, as shown in Figure 1. Most of the tunnel body is positioned within silt and silty soil, while the base of the tunnel rests in a comparatively hard residual soil layer. Above the tunnel, an intercity expressway has undergone multiple reclamation processes due to uneven settlement of the soft soil. This has caused continuous consolidation and settlement of the silt layer and an amplified soil weight over the tunnel, inducing significant lateral deformation. The soft silt layer struggles to provide sufficient lateral support for the shield tunnel structure, which leads to excessive lateral deformation. Such distortion in shield tunnels frequently results in joint leakage and even structural issues such as tunnel concrete segment cracking and collapse, compromising the structural integrity and safety of passing trains.

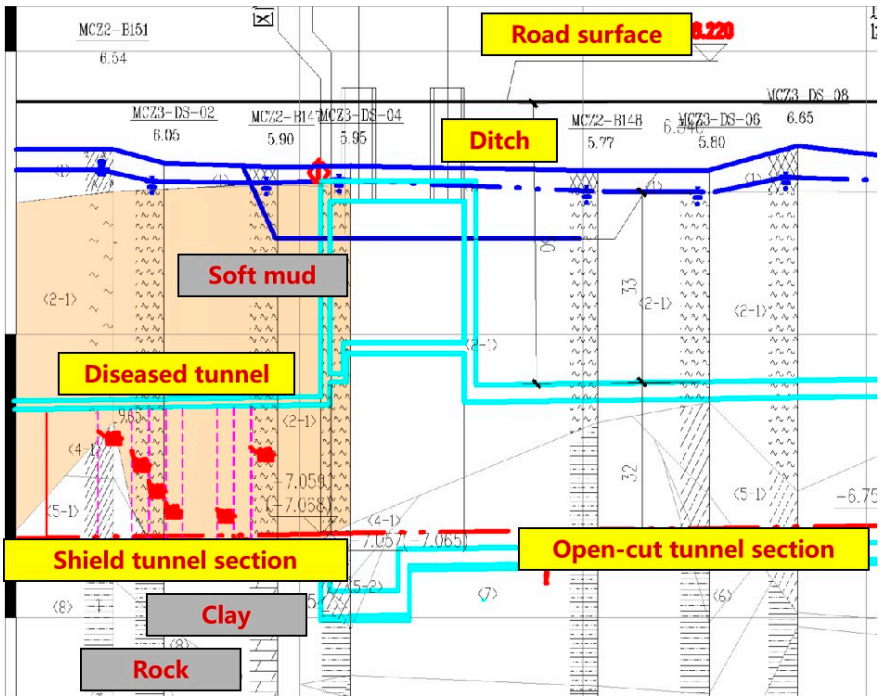

Figure 1. Cross-section of the defected tunnel and the stratum in which it is located.

2.2. Analysis of Monitoring Data

The tunnel commenced operations in December 2006. By the first half of 2020, many rings of tunnel lining segment in the tunnel's left and right lines exhibited widespread and numerous cracks. The most pronounced cracking was observed in ring No. 7 of the upline, as depicted in Figure 2.

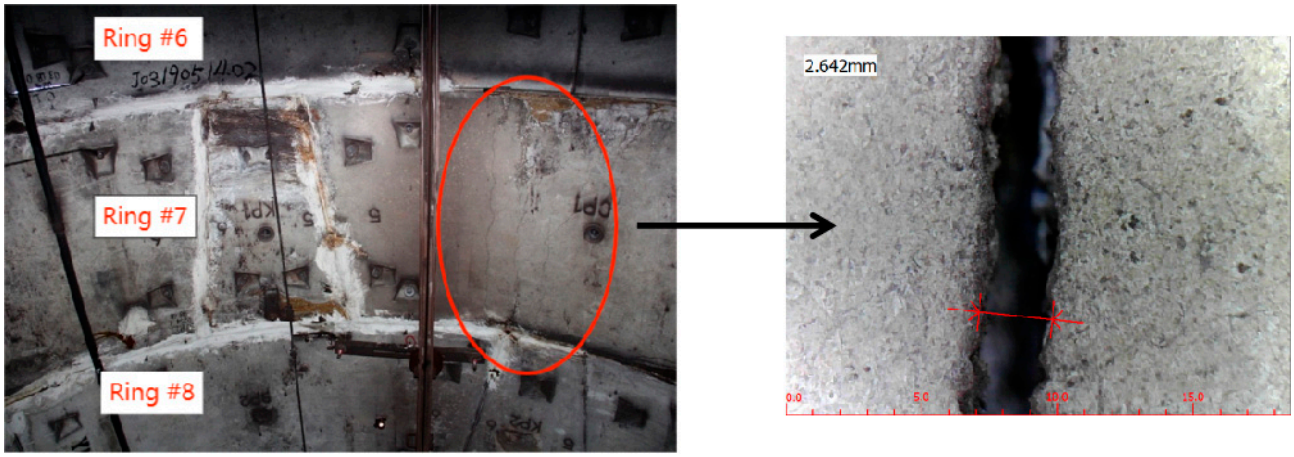

Figure 2. Crack map of ring 7 on the upstream line.

After detecting significant issues in the shield tunnels, laser scanning was employed for monitoring tunnel deformation. The ellipticity monitoring method predominantly uses the GRP5000 mobile laser scanning measurement system for continuous scanning of underground shield tunnels. This approach captures holographic images and data within the specified tunnel section, encompassing tunnel section ellipticity in each ring, vehicle limits, and the tubular segment's surface disease, among other metrics.

Ellipticity is derived from the tunnel's deformed short and long axes and is typically determined by the difference between a tunnel's maximum and minimum diameters and its designed internal diameter, expressed in thousandths as a ratio. Since limited research currently exists on the lateral deformation limit of relevant tunnels based on ellipticity, engineering experience generally sets this threshold at 25‰. The latest monitoring results prior to reinforcement measures are presented in Figure 3.

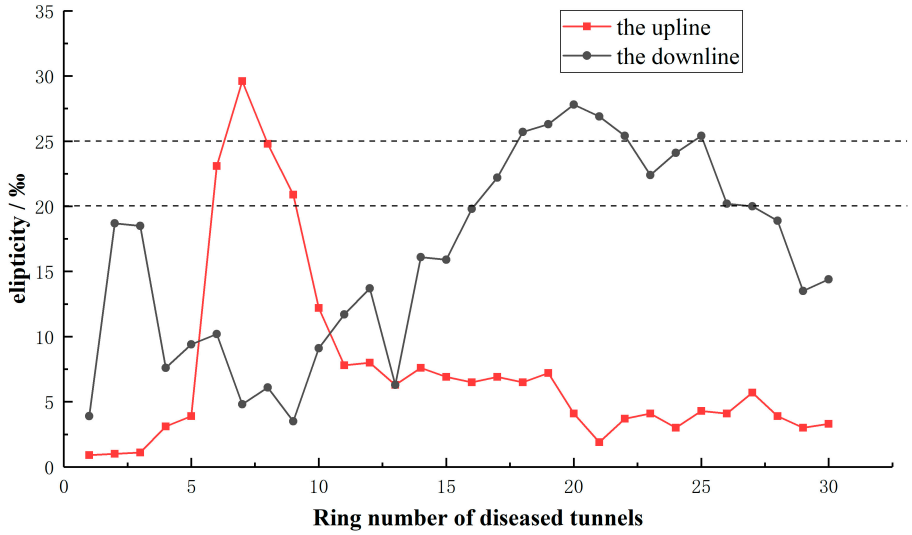

Figure 3. Ellipticity monitoring values of tunnels in cases of defective intervals.

Multiple shield tunnel rings in the upline and downline of this interval exhibited lateral deformations exceeding the empirical 25‰ limit. Specifically, the maximum elliptic deformation on the upline reached 30.9‰ in one ring, while on the downline, it was 27.8‰, impacting six rings. In addition, the uplines and downlines did not exhibit identical mileage regarding the over-limit deformation rings. The deficiency locations were approximately 20 m apart horizontally. Adjacent tunnel rings showing over-limit deformation demonstrated apparent structural issues. Ring No. 7 in the upstream line experienced the most pronounced elliptic deformation at 30.9‰, with the most extensive crack measuring around 2.64 mm.

Several observations can be made based on the disease distribution map from Figure 4 and comprehensive tunnel cracking data from Table 1. There is a relationship between the number of shield tunnel cracks, crack width, and tunnel lateral deformation. Shield tunnels are prone to cracking when the ellipticity is large, and the larger the ellipticity, the larger the number and width of cracks are likely to be. At the same time, even when tunnel deformation is minimal, multiple minor cracks can appear. Some shield ring deformations exceeding the general 25‰ limit did not exhibit apparent cracks. However, the location of these cracks is consistent, predominantly at the top of the shield tunnel ring, with the crack direction mainly being longitudinal. The tunnel's waist sides are susceptible to leakage and other structural issues. According to the Design Code for Concrete Structures GB50010-2010 (2015 Edition) specifications [18], the width of concrete cracks can be estimated using the following Equations (1)–(5):

$$\omega_{\max} = \alpha_{cr}\psi\frac{\sigma_s}{E_S}\left(1.9c_s + 0.08\frac{d_{eq}}{\rho_{te}}\right), \tag{1}$$

$$\psi = 1.1 - 0.65\frac{f_{tk}}{\rho_{te}\sigma_s}, \tag{2}$$

$$d_{eq} = \frac{\sum n_i d_i^2}{\sum n_i v_i d_i}, \tag{3}$$

and

$$\rho_{te} = \frac{A_s + A_p}{A_{te}}, \tag{4}$$

where $\omega_{\max}$ is the maximum crack width affected by the long-term effects.

The tensile stress in the tension zone can be derived using the following equation for the concrete segmental lining's bending components.

$$\sigma_{sq} = \frac{M_q}{0.87h_0A_s}. \tag{5}$$

Based on the tunnel construction drawings, the design parameters are as follows: the tunnel segment width b is 1500 mm; the tunnel segment thickness h is 300 mm; the protective layer thickness c_s is 35 mm; the reinforcement area A_s is 2383 mm^2; the prestressed reinforcement area A_P is 0; the modulus of elasticity of reinforcement E_S is 200,000 N/mm^2; the effective height of the cross-section h_0 is 257 mm; the standardized value of concrete strength f_{tk} is 2.64 N/mm^2; the characteristic coefficient of force for eccentrically compressed members α_{cr} is 1.9; the effective tensile concrete cross-section area A_{te} is 225,000 mm; the nominal diameter of the ith longitudinal reinforcement is d_i; the number of roots of the ith longitudinal reinforcement is n_i; the relative bond characteristic coefficient of the longitudinal reinforcement v_i is 1.0; the equivalent diameter of reinforcement d_{eq} is 15.98 mm; the moment of the tunnel is M; the reinforcement stress is σ_s; and the reinforcement's yield strength is 335 MPa.

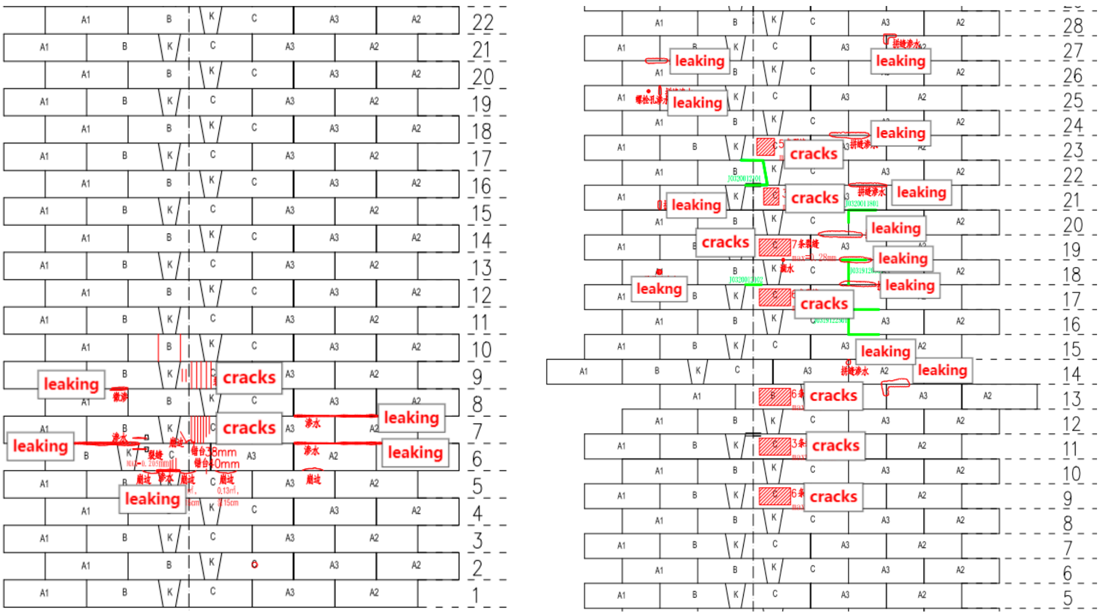

(a) Upline (b) Downline

Figure 4. Expanded view of the defective case.

Table 1. Comprehensive information on tunnel cracking in an interval.

Upline:				
Mileage (m)	**Ring Number**	**Tunnel Defect Statistics**	**Maximum Crack Width (mm)**	**Current Ellipticity of the Tunnel (‰)**
15,197	5	No cracks seen		4.8
15,195.5	6	3 Short cracks without penetration at the top	0.205	23.1
15,194	7	8 Cracks through the top	2.642	30.9
15,192.5	8	No cracks seen		24.8
15,191	9	6 Cracks through the top	0.615	11.3
15,189.5	10	No cracks seen		12.4
Downline:				
Mileage (m)	**Ring Number**	**Tunnel Defect Statistics**	**Maximum Crack Width (mm)**	**Current Ellipticity of the Tunnel (‰)**
15,191	9	No cracks seen		3.5
15,189.5	10	6 Cracks through the top	0.212	9.1
15,188	11	No cracks seen		11.7
15,186.5	12	3 Top penetration cracks	0.220	13.7
15,185	13	No cracks seen		6.3
15,183.5	14	6 Cracks through the top	0.304	16.1
15,182	15	No cracks seen		15.9
15,180.5	16	No cracks seen		19.8
15,179	17	No cracks seen		22.2
15,177.5	18	6 Cracks through the top	1.222	25.7
15,176	19	No cracks seen		26.3
15,174.5	20	7 Top penetration cracks	0.283	27.8
15,173	21	No cracks seen		26.9
15,171.5	22	3 Top penetration cracks	0.231	25.4
15,170	23	No cracks seen		22.4
15,168.5	24	5 Top penetration cracks	0.174	24.1
15,167	25	No cracks seen		25.4
15,165.5	26	No cracks seen		20.2
15,164	27	No cracks seen		20.0

Given the formula above, if the crack width of the tunnel segment ω_{max1} exceeds 0.30 mm, the reinforcement stress surpasses the design value for reinforcement strength. In addition, the tensile reinforcement yields when the crack width ω_{max2} exceeds 0.37 mm. Based on these calculations, there are two tunnel rings in the upstream line with crack widths exceeding 0.37 mm, causing the reinforcement in these areas to yield under tension. Conversely, in the downstream line, one ring has a crack width exceeding 0.37 mm, and another possesses a crack width larger than 0.30 mm but not exceeding 0.37 mm.

2.3. Tunnel Reinforcement and Subsequent Monitoring Data Analysis

In response to these findings, the relevant departments initiated a special reinforcement project. The specific steel plate reinforcement method for the affected tunnel includes the following steps: firstly, repairing the tunnel segment cracks in the tunnel; secondly, pasting aramid fiber cloth to the cracks, ensuring joint stress between the shield tunnel segment and the aramid fibers; and lastly, introducing an additional steel plate inside the tunnel as a structural reinforcement measure, enabling the combination of the steel plate and the shield tunnel segment to establish a composite structure. In order to guarantee the tunnel's structural integrity during the routine operation of the reinforced tunnel, it is imperative to periodically monitor the deformation and internal forces of the reinforced composite structure. Due to space limitations, only the results from ring No. 7 of the upstream line, which exhibits the highest ellipticity and most significant damage, are displayed. High-precision vibrating string surface strain gauges facilitate this monitoring, with stress-strain monitoring points positioned in five directions within each tunnel ring section. The variations in internal force at each point within the reinforced composite structure of ring No. 7 over time are depicted in Figure 5.

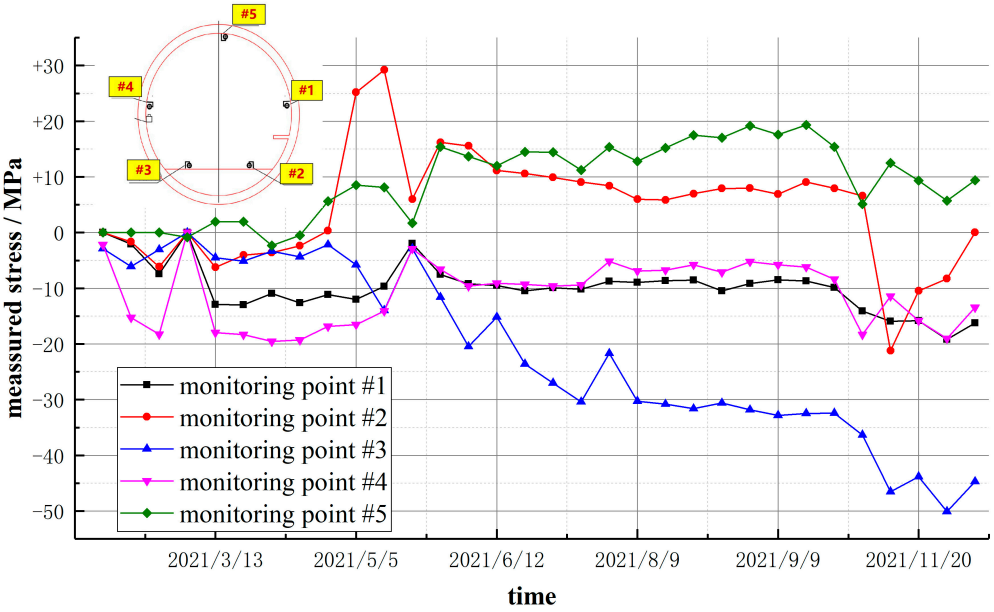

Figure 5. Ring 7 of the uplink. Note: the positive stress value indicates tensile, while the negative value indicates compressive.

During the first year after the reinforcement of the shield tunnel with steel plates, the subway tunnel operated normally. Figure 5 illustrates that the overall bearing characteristics of the concrete tunnel-steel plate composite structure remain relatively stable. Although some measurement points display minor stress fluctuations due to external influences, the overall stress level remains minimal. The monitoring data accounts not only for changes in the internal force of the composite structure but also monitors the tunnel's transverse deformation, settlement, and other parameters. All these values remain within 3 mm, indicating minimal deformation and confirming that they are within the safe range.

This data underscores that the structure remained safe and stable throughout the period following the reinforcement.

2.4. Summary of Engineering Cases

The deformation limit, grounded in ellipticity, varies among cities due to stratigraphic differences and distinct design parameters of shield tunnels. Typically, this limit ranges between 20‰ and 25‰ based on empirical data. Determining whether a tunnel's lateral deformation exceeds this threshold and consequently indicates a decrease in bearing capacity or the presence of structural issues requires careful assessment. In the case discussed in this study, the shield tunnel's maximum ellipticity reached about 30‰ before reinforcement, showing clear structural problems. However, other tunnels with elliptic deformation exceeding 20–25‰ displayed no detectable structural damage. In contrast, tunnels with minor lateral deformation can still present issues such as cracks or leaks. Therefore, the steel-concrete composite structure remains stable after reinforcing tunnels showing signs of deterioration or excessive deformation. This demonstrates the effectiveness of the steel plate reinforcement method for damaged shield tunnels. However, the indiscriminate application of steel plate reinforcement is not recommended. Beyond its significant cost, the construction process can disrupt the tunnel structure's stability. Therefore, establishing appropriate deformation limits for shield tunnels, considering varied external conditions, is essential. To assist in developing this standard, this study employs finite-element analysis based on the discussed engineering case.

3. Finite-Element Analysis

3.1. Material Structural Modeling and Parameters

This research utilizes general finite-element analysis software, Midas FEA NX 1.0, to develop the finite-element model of the shield tunnel's segment. Load simulations are performed on the three-dimensional finite-element model. Material specifications, bolt quantities and strengths, and reinforcement measures are chosen based on real-world scenarios. The concrete grade used for the shield tunnel is C50, employing the concrete plastic damage intrinsic model. The damage factor can determine the material's elastic modulus E once the concrete undergoes plastic damage.

$$E = (1 - d_k)E_0$$

where E_0 is the initial modulus of elasticity of the material and d_k is the concrete damage factor, which can be expressed as the damage parameter of concrete in tension or compression, respectively.

Stress-strain curves for concrete's uniaxial tensile and compressive conditions can be inferred from calculations in line with the concrete code [18]. The energy equivalent model determines the damage parameter d [19]. Two key plastic damage factors of C50 concrete are shown in Figure 6.

3.2. Model Boundary Processing

The model incorporates three-dimensional curved bolts and bolt handholes to simulate the contact relationship between concrete segments, bolts, and handholes. The size and relative positioning derive from construction design drawings. To reflect the yielding behavior of the steel, the Von Mises eigenstructure is used for the connecting bolts. The yield strength of 5.8-grade bolts used in this model is taken as 400 MPa, and the ultimate strength is taken as 500 MPa. The contact points between adjacent segments, bolts, and tunnel segments employ a surface-to-surface contact model. This model enforces hard contact in the normal direction, allowing pressure transfer and separation post-contact, and the tangential direction is modeled using the Coulomb friction method based on the penalty function approach. The finite-element model is shown in Figure 7.

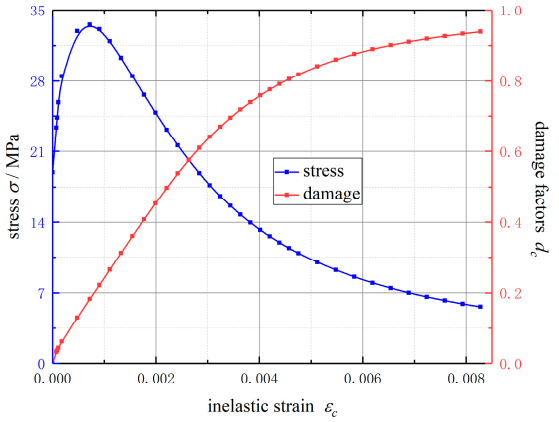

Compressive inelastic strain, stress, and damage factor curves

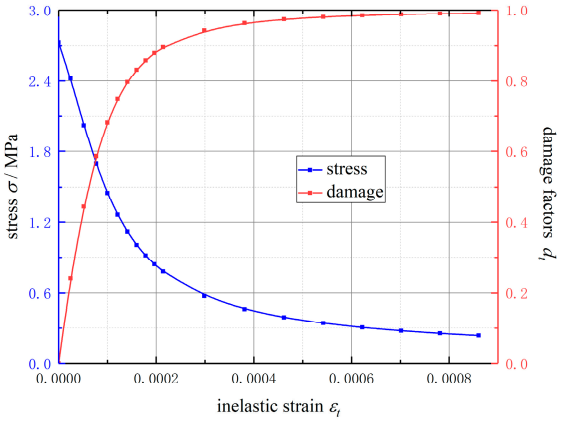

Tensile inelastic strain, stress, and damage factor curves

Figure 6. Plastic damage factor of C50 concrete.

Figure 7. Schematic diagram of the finite-element model of the shield tunnel.

The surrounding rock's constraint on the tunnel segment's exterior is simulated using curved springs. The foundation reaction coefficients for the radial springs can be sourced from the table in accordance with the standard penetration strikes of the strata [20], or they can be determined using established empirical values or calculated per theoretical methods [21,22]. This research focuses on prevalent stratigraphic parameters in South China, choosing various foundation spring coefficients to represent common soil strata. Foundation spring coefficients of 5, 10, 20, and 30 MPa/m are applied, loading each instance based on real-world deformation. The remaining two tangential spring foundation reaction force coefficients are 1/3 of the radial coefficients [23].

3.3. Loading Methods and Validation

Given the intricacies of actual engineering challenges, it is suggested to use the convergence of the tunnel's vertical and lateral deformation from real monitoring data as the target for the numerical simulation of the shield tunnel structure. This involves incrementally increasing vertical pressure while maintaining lateral pressure at 0.5 times the vertical pressure, subsequently analyzing the tunnel structure's safety under specific ellipticity while ensuring a reasonable load state. Based on the model calibration from the

literature [24], the shield tunnel undergoes modeling and analysis. Model parameters are adjusted dynamically, comparing results such as internal force, convergence deformation, and concrete cracking to foot-scale test models. This process confirms the accuracy and applicability of the developed finite-element model and provides essential model parameters for further simulation and analysis. The full-scale model test of a shield segment in the literature [24] is shown in Figure 8, and the schematic diagram of the loading of the validation model in Figure 9.

Figure 8. Full-scale model test of shield segment in the literature [24].

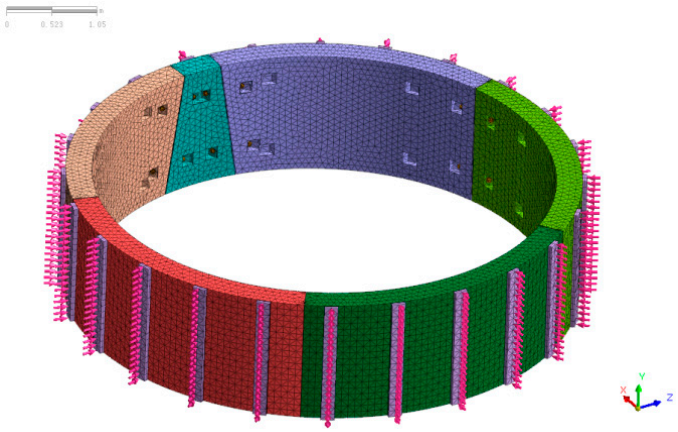

Figure 9. Schematic diagram of the loading of the validation model.

3.4. Shield Tunnel Loading Results

In Figure 10, the blue color signifies that the structure remains in the elastic stage, corresponding to a damage value of 0. In this region, the unit remains in the elastic stress stage, and the unit stress is below the elastic limit stress of the concrete plastic damage constitutive model. Regions other than blue suggest that the unit is in the plastic stage, with damage values ranging between 0 and 1. A higher value indicates more severe damage within that specific structural region.

For varying foundation parameters, denoted as k, even under approximate deformation conditions, the damage inside the tunnel segment for the erroneous seam tunnel consistently occurs in the same location. This consistency is due to the regularity observed in the structural loading damage results. This analysis focuses on the foundation spring coefficient set to 10 MPa/m. When the ellipticity ranges between 10‰ and 15‰, the concrete in the tensile zone displays almost identical cracks. The tunnel's top is susceptible

to cracks, while excessive deformation at the tunnel's waist can result in localized pressure collapse, manifesting as a block collapse phenomenon. The exterior of the tunnel's waist is also susceptible to damage. Although damage to the outside of the tunnel is not readily observable, it may still lead to leakage from the waist side of the tunnel and even corrosion of exposed reinforcement.

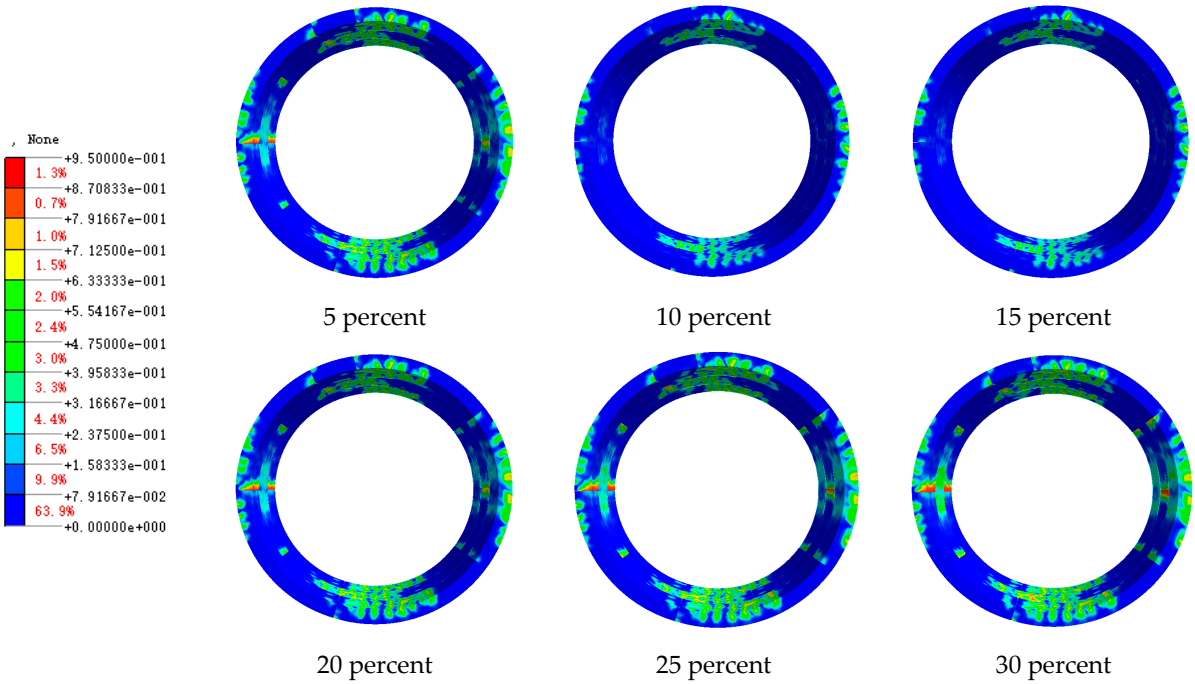

Figure 10. Damage cloud (perspective view) of the tunnel segment with ellipticity development when the foundation spring coefficient is taken as 10 MPa/m.

Figures 11–13 show that a critical distinction between the algorithms is the overall yield point of the structure during loading. Analyzing the loading-deformation curve, a significant slope change in the curve indicates a decrease in the loaded stiffness, implying that the entire ring structure is in the yielding stage. For a k value of 5, 10, 20, and 30 MPa/m, the yielding begins when horizontal convergence reaches roughly 90, 80, 70, and 60 mm, respectively.

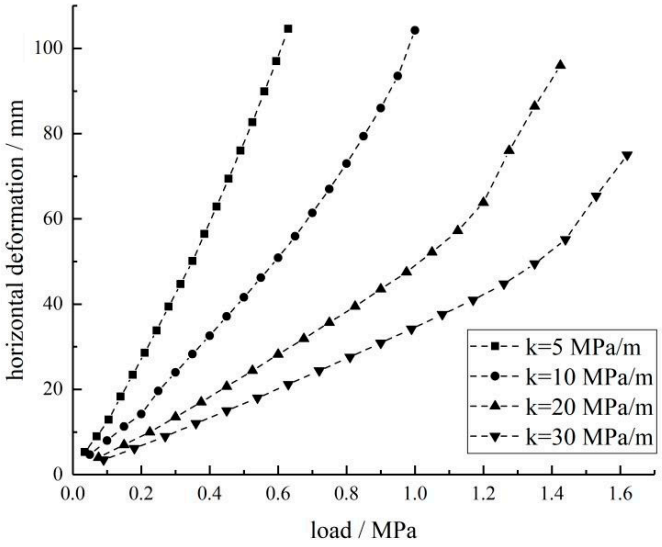

Figure 11. Vertical load-horizontal convergence values with different ground resistance coefficients.

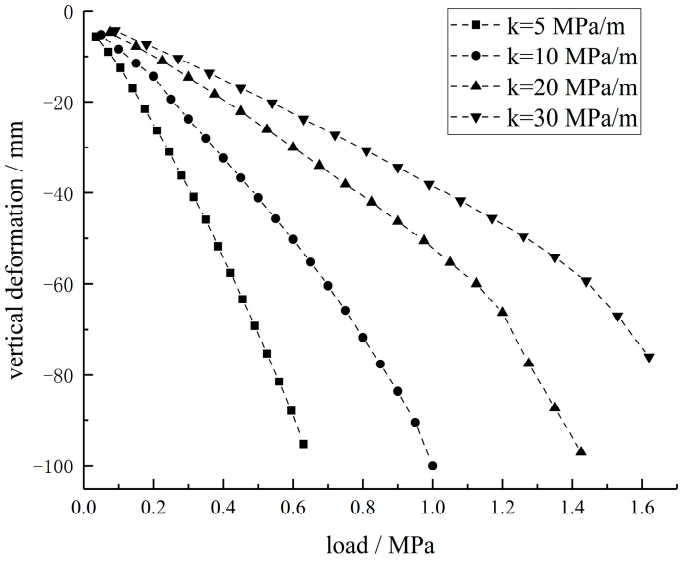

Figure 12. Vertical load-vertical convergence values with different ground resistance coefficients.

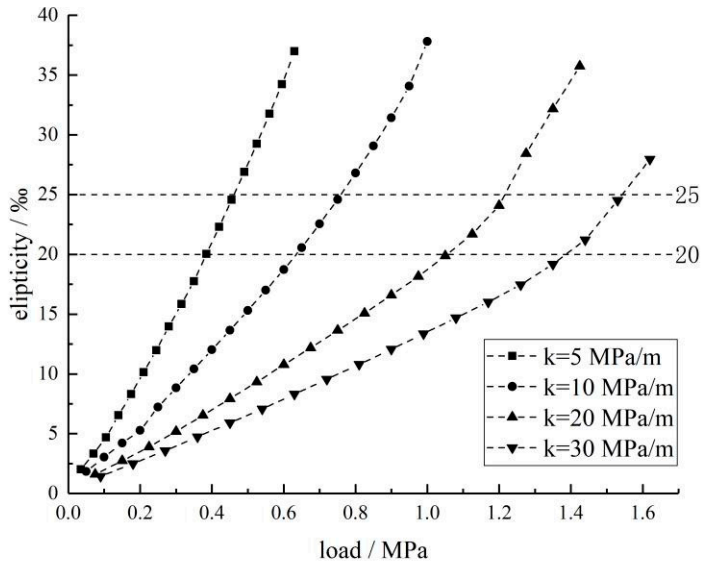

Figure 13. Vertical load-ellipticity curve.

Figure 14 depicts the damage cloud diagram for each scenario at an ellipticity of 25‰. With smaller k values, the red region in the arch waist is minimized, indicating lesser damage and the structure's ability to bear the normal load. Conversely, larger k values lead to pronounced damage in the arch waist. Comparing this with the loading curve reveals that the structure is almost in the yielding phase.

In summary, under symmetrical loading conditions, an increase in vertical loading exposes the arch's inner side as the most vulnerable region due to concrete tension-induced cracks. However, the arch's base, linked to the roadbed, does not demand significant damage monitoring. Stratigraphic conditions considerably restrict the lateral deformation of the tunnel segments.

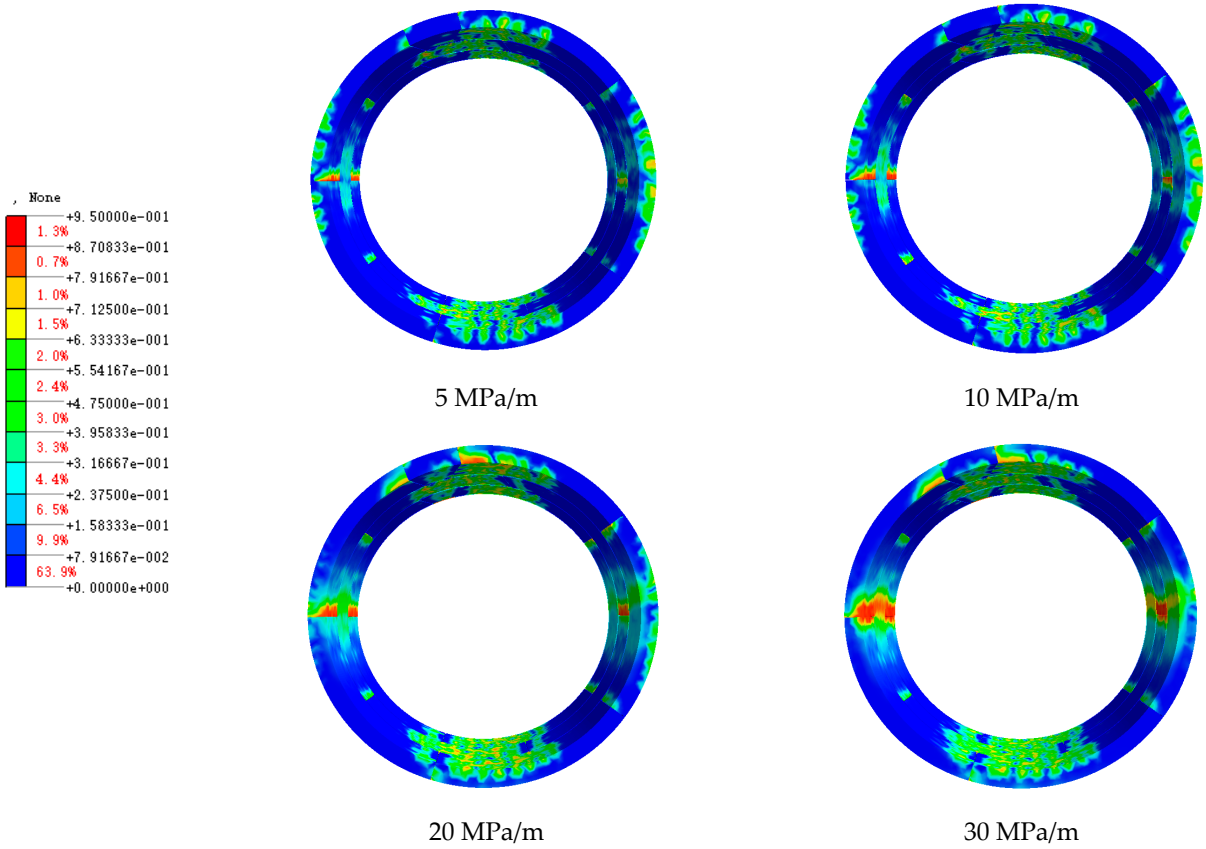

Figure 14. Damage cloud (perspective view) of tunnel segments at an ellipticity of 25‰.

3.5. Loading Results for Bolts and Reinforcement

The Guangzhou subway tunnel, as discussed in this study, employs 5.8-grade high-strength bolts with a yield strength of approximately 400 MPa. Figure 15 shows that when the ellipticity approaches 30‰, the bolts at the joints with the most significant deformation begin to yield. After the bolts at the top joints yield, the connecting bolts at the waist-part joints also enter the yielding stage as deformation increases. Through loading simulation, for soft soil regions, tunnel segment deformation primarily arises from joint deformation. The connecting bolts might yield tension due to the excessive opening of the tunnel segment joints. Conversely, in hard rock areas with significant stratigraphic restriction, tunnel segment joint deformation is minimal. Deformation mainly results from the softening and cracking of the concrete tunnel segment, and the bolts are less likely to experience substantial stresses. The discrepancy in bolt stress under varied surrounding rock conditions might not be stark, but it does illustrate the deformation characteristics of the shield tunnel structure.

Regarding the impact of the reinforcement ratio on the shield tunnel's lateral deformation, numerical models indicate that the tunnel segment's lateral deformation primarily stems from joint deformation. This causes the tunnel segment to exhibit a "transverse duck-egg" deformation pattern. Within a reasonable reinforcement ratio, increasing this ratio enhances the ultimate load-carrying capacity and crack resistance of the tunnel segment. However, it minimally affects the local mechanical behavior of the joints and the tunnel segment's overall deformation stiffness. The reinforcement ratio's influence on the entire ring's bearing capacity is less pronounced than its impact on the tunnel segment's bearing performance. In general, the bolts and tunnel segment reinforcement affect the entire ring of segment's ultimate load-carrying capacity but minimally influence the overall deformation pattern of the tunnel segment and the establishment of generalized lateral deformation limits for tunnels.

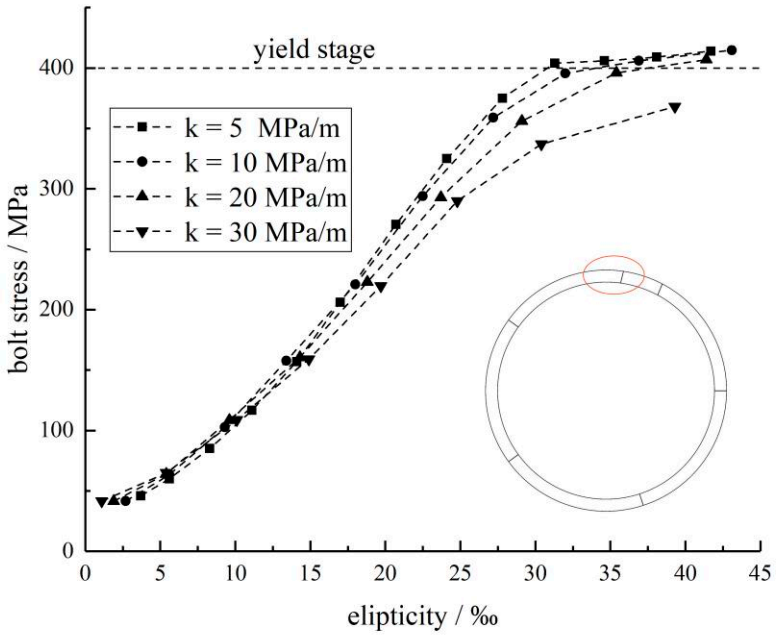

Figure 15. Variation curve of bolt stress with increasing ellipticity.

4. Development of Lateral Deformation Limits for Shield Tunnels

Analyzing structural bearing capacity reveals that when the foundation spring coefficient is 30 MPa/m, the tunnel nears yielding at an ellipticity of 20‰. However, when the coefficient is 5 MPa/m, there is no clear yielding even when the tunnel's ellipticity exceeds 35‰. This suggests that a higher foundation spring coefficient results in reduced tunnel deformation corresponding to structural deformation when the tunnel yields entirely. From a safety perspective, excessive lateral deformation can diminish the tunnel's sectional headroom, potentially endangering ceiling equipment within the tunnel and posing threats to moving trains. In addition, such deformation can lead to roadbed unevenness, necessitating slowed train movement.

Factors such as the tunnel design parameters, surrounding ground conditions, existing issues, and deformation safety margin reservations should be integrated to limit the precast concrete tunnel segment's lateral deformation in the metro shield tunnels. Excessive elliptical deformation in shield tunnels irreparably damages concrete structures. Large lateral deformations from external loading, even if promptly unloaded, make it challenging to rectify the tunnel segment's lateral deformation [25]. This directly affects the safety margin for enduring structures like shield tunnel structures. Hence, the shield tunnel damage treatment principle should be: thoroughly inspect and address potential issues surrounding the tunnel early during deformation. The structure should be reinforced if deformation continues to grow post-inspection and shows no convergence signs.

Considering the actual conditions, the standard warning value for lateral deformation based on the ellipticity evaluation of the Guangzhou Metro shield tunnels must be 20‰, and the control value at 25‰. Depending on various foundation spring coefficients, the finite-element simulation results for the shield tunnel, considering increasing lateral deformation of structural damage, are listed in Tables 2 and 3.

When the tunnel's single-ring elliptic variation reaches 15–20‰, the relevant departments overseeing subway protection must monitor the interval along the tunnel more closely and investigate whether engineering activities surrounding the tunnel can seriously impact its structural safety. If the tunnel's single-ring elliptic variation reaches 25‰ and the adjacent multi-ring tunnel segment ellipticity is 20‰ or more, and continuous monitoring results indicate that the deformation lacks a convergence trend and the tunnel interior exhibits signs of cracking, seepage, or crumbling blocks, then timely measures are necessary to reinforce the tunnel within the damage interval. In addition, for shield tunnels in hard

surrounding rock, the deformation control value should be adjusted in accordance with the standards mentioned above. The above safety limits and the corresponding safety control levels under the corresponding deformation states can be applied to judge the safety state of a 6-m diameter jointed metro shield tunnel. This study mainly focuses on 6-m diameter shield tunnels. Future research could be conducted on deformation control criteria for shield tunnels of different diameters.

Table 2. Safety and health status control levels of subway shield tunnels.

Control Level	Gauge
I	Normal service and good performance
II	Beginning of cracks and leaks in a working condition with micro-cracks
III	Cracks and leaks have further increased, requiring increased attention and health monitoring
IV	Further deterioration of structural cracking, severe leakage from adjacent rings, urgent need for reinforcement
V	The whole ring structure will start to yield, and the loaded stiffness will decrease significantly

Table 3. Corresponding levels of safety limits for lateral deformation in metro shield tunnels.

Convergent Deformation	<30 mm	30–40 mm	40–55 mm	55–70 mm	70–85 mm	>85 mm
Ellipticity	**<10‰**	**10–15‰**	**15–20‰**	**20–25‰**	**25–30‰**	**>30‰**
k = 5 MPa/m	I	II	III	III	IV	IV, V
k = 10 MPa/m	I	II	III	III	IV	IV, V
k = 20 MPa/m	I, II	III	III	III	IV	V
k = 30 MPa/m	I, II	III	III	IV	V	V

5. Conclusions

This study evaluates damage emergence and reinforcement of a case with significant lateral deformation in the Guangzhou Metro. It also suggests structural safety limits for the ellipticity, drawing from a three-dimensional refined finite-element model analysis of the shield tunnel segment. The following conclusions are drawn:

1. The circular shield is most susceptible to cracking based on both observed cases and finite-element model loading results. This vulnerability is most visible from the inside, specifically within the arch. When the tunnel is located in a weak stratum, the arch's interior waist is more likely to experience joint compression collapse. The stratum conditions can significantly restrict the lateral deformation of the tunnel segment.
2. The variance in bolt stress across different surrounding rock conditions is minimal within the finite-element simulation. However, this difference underscores the deformation characteristics of the shield tunnel structure. The reinforcement ratio has a lesser effect on the bearing capacity of the entire ring compared to a single piece of the segment. Consequently, neither significantly impacts the segment's overall deformation trend or the establishment of deformation limit values.
3. The steel plate reinforcement technique proves highly effective in reinforcing shield tunnels with extensive elliptical variations. Monitoring data affirms that, post-reinforcement, the entire structure remains safe and stable during regular operations for an extended period.
4. Determining appropriate deformation limit values for varying external conditions of the shield tunnel is crucial. When integrated with real-world conditions, the Guangzhou Metro shield tunnel's ellipticity-based lateral deformation warning value is set at 20‰, with the control value at 25‰. The deformation control value should be adjusted based on the criteria above if the tunnel lies within a hard soil layer.

Author Contributions: S.K.: conceptualization, review, and editing; J.C.: methodology and writing the original draft.; Y.L. and Y.W.: data curation; H.Z.: software and validation. All authors have read and agreed to the published version of the manuscript.

Funding: This research was funded by the Guangdong Provincial Key Laboratory of New Technology in Urban Rail Transit Engineering Construction (2017B030302009) and the Guangzhou Academician Expert Workstation (2021CXZX030).

Institutional Review Board Statement: Not applicable.

Informed Consent Statement: Not applicable.

Data Availability Statement: Data are contained within the article.

Conflicts of Interest: Authors Shaode Kan, Yuehua Liang and Yizhao Wang were employed by the company Guangzhou Metro Design & Research Institute Co., Ltd. The remaining authors declare that the research was conducted in the absence of any commercial or financial relationships that could be construed as a potential conflict of interest.

References

1. Beard, A.N. Tunnel safety, risk assessment and decision-making. *Tunn. Undergr. Space Technol.* **2010**, *25*, 91–94. [CrossRef]
2. Ma, L.; Luo, H.B.; Chen, H.R. Safety risk analysis based on a geotechnical instrumentation data warehouse in metro tunnel project. *Autom. Constr.* **2013**, *34*, 75–84. [CrossRef]
3. Vinoth, M.; Aswathy, M.S. Behaviour of existing tunnel due to adjacent deep excavation—A review. *Int. J. Geotech. Eng.* **2022**, *16*, 1132–1151. [CrossRef]
4. Zhang, D.M.; Xie, X.C.; Li, Z.L.; Zhang, J. Simplified analysis method for predicting the influence of deep excavation on existing tunnels. *Comput. Geotech.* **2020**, *121*, 103477. [CrossRef]
5. Bian, X.; Hu, H.; Zhao, C.; Ye, J.; Chen, Y. Protective effect of partition excavations of a large-deep foundation pit on adjacent tunnels in soft soils: A case study. *Bull. Eng. Geol. Environ.* **2021**, *80*, 5693–5707. [CrossRef]
6. Lediaev, A.P.; Konkov, A.N.; Novikov, A.L.; Soloviev, D.A. Influence evaluation of buildings constructed in protected zone on st.petersburg subway underground structures stress-strain state. *Proscedia Eng.* **2017**, *189*, 492–499. [CrossRef]
7. Wu, H.N.; Shen, S.L.; Yang, J.; Zhou, A.N. Soil-tunnel interaction modelling for shield tunnels considering shearing dislocation in longitudinal joints. *Tunn. Undergr. Space Technol.* **2018**, *78*, 168–177. [CrossRef]
8. Xiao, T.; Zhang, L.M.; Li, X.Y.; Li, D. Probabilistic stratification modeling in geotechnical site characterization. *ASCE ASME J. Risk Uncertain Eng. Syst. A* **2017**, *3*, 04017019. [CrossRef]
9. Wang, X.; Li, Z.; Wang, H.; Rong, Q.; Liang, R.Y. Probabilistic analysis of shield-driven tunnel in multiple strata considering stratigraphic uncertainty. *Struct. Saf.* **2016**, *62*, 88–100. [CrossRef]
10. Yamamoto, K.; Lyamin, A.V.; Wilson, D.W.; Sloan, S.W.; Abbo, A.J. Stability of a circular tunnel in cohesive-frictional soil subjected to surcharge loading. *Comput. Geotech.* **2011**, *38*, 504–514. [CrossRef]
11. Yamamoto, K.; Lyamin, A.V.; Wilson, D.W.; Sloan, S.W.; Abbo, A.J. Stability of dual circular tunnels in cohesive-frictional soil subjected to surcharge loading. *Comput. Geotech.* **2013**, *50*, 41–54. [CrossRef]
12. Shi, C.; Cao, C.; Lei, M.; Peng, L.; Ai, H. Effects of lateral unloading on the mechanical and deformation performance of shield tunnel segment joints. *Tunnelling Undergr. Space Technol.* **2016**, *51*, 175–188. [CrossRef]
13. Tian, L.G.; Hu, Z.Q.; Chen, J. Experimental and numerical research on defective shield segment under cyclic loading. *Shock Vib.* **2021**, *12*, 8567899. [CrossRef]
14. Su, D.; Chen, W.J.; Wang, X.T.; Huang, M.L.; Pang, X.C.; Chen, X.S. Numerical study on transverse deformation characteristics of shield tunnel subject to local soil loosening. *Undergr. Space* **2022**, *7*, 106–121. [CrossRef]
15. Nematollahi, M.; Molladavoodi, H.; Dias, D. Three dimensional numerical simulation of the shiraz subway second line—Influence of the segmental joints geometry and of the lagging distance between twin tunnels' faces. *Eur. J. Environ. Civil Eng.* **2018**, *24*, 2116–7214. [CrossRef]
16. Liu, J.; Shi, C.; Lei, M.; Wang, Z.; Cao, C.; Lin, Y. A study on damage mechanism modelling of shield tunnel under unloading based on damage-plasticity model of concrete. *Eng. Fail. Anal.* **2021**, *123*, 105261. [CrossRef]
17. Wang, F.; Huang, H.; Soga, K.; Li, Z. 3D modelling of concrete tunnel segmental joints and the development of a new bolt-spring model. *Tunnelling Undergr. Space Technol.* **2021**, *110*, 103835. [CrossRef]
18. *GB 50010-2010[S]*; Code for Design of Concrete Structures. China Architecture & Building Press: Beijing, China, 2010.
19. Newman, G.U. The continuous damage theory of brittle materials. *J. Appl. Mech.* **1998**, *48*, 809–815.
20. The Japanese Geoteohnioal Society. *From Investigation and Design to Construction of Shield Construction Method*; The Japanese Geoteohnioal Society: Tokyo, Japan, 1997. (In Japanese)
21. Wood, A.M.M. The circular tunnel in elastic ground. *Géotechnique* **1975**, *25*, 115–127. [CrossRef]
22. Plizzari, G.A.; Tiberti, G. Steel fibers as reinforcement for precast tunnel segments. *Tunnelling Undergr. Space Technol.* **2006**, *21*, 438–439. [CrossRef]

23. Koyama, Y. Present status and technology of shield tunneling method in Japan. *Tunn. Undergr. Space Technol.* **2003**, *18*, 145–159. [CrossRef]
24. Lv, Y. *Full-Scale Model Test of Shield Tunnel Segment and Simulation Analysis of Circumferential Joint*; China Academy of Railway Sciences: Beijing, China, 2019.
25. Liu, T.J.; Chen, S.W.; Liu, H.Y. Deformation characterization and distress diagnosis of a metro shield tunnel by adjacent constructions. *Adv. Civ. Eng.* **2020**, *2020*, 4216349.